

# Study of the influence of Semi-porous baffles on the three-phase separation efficiency in a horizontal separator vessel via CFD

Jéssica Barbosa da Silva do Nascimento<sup>1\*</sup>, Alysson Dantas Ferreira<sup>2†</sup>, Angela Lucinia Urtiga Vasconcelos<sup>3†</sup> and Severino Rodrigues de Farias Neto<sup>2†</sup>

*1\*Chemical Engineering, UESC, Rodovia Jorge Amado, km 16, Ilhéus, 45662-900, BA, Brazil.*

*2\*Process Engineering, UFCG, Aprigio Veloso, 882, Campina Grande, 58429-900, PB, Brazil.*

*3\*Sugar and Alcohol Technology, UFPB, Rua dos Escoteiros, s/n, João Pessoa, 58058-600, PB, Brazil.*

\*Corresponding author(s). E-mail(s): jbsnascimento@uesc.br;

Contributing authors: alysson.dantas@eq.ufcg.edu.br; angela.vasconcelos@academico.ufpb.br; s.fariasn@gmail.com;

## Abstract

Horizontal separator vessels exhibit better phase separation efficiencies when fluids flow at lower velocities, favoring the sedimentation process. The optimized determination of internal devices such as baffles can reduce fluid velocity from the inlet to the separation region. This research aimed to evaluate the impact of semi-perforated baffles on flow dynamics and the separation efficiency of gas, oil, and water in a three-phase horizontal separator vessel. To achieve this goal, a base geometry was adapted. Two configurations of semi-perforated baffles were analyzed, varying their distance from the inlet, height relative to the vessel bottom, and vertical length. Computational fluid dynamics was the tool used to obtain numerical results. The multiphase flow was modeled using the VOF model in conjunction with the standard k-epsilon turbulence model. The results indicated that the insertion of baffles contributed to attenuating the velocity of the inlet fluids. Among the analyzed geometric arrangements, it can be concluded that the three-phase horizontal separator with a semi-perforated baffle at position P1 exhibited a more uniform three-phase flow and better liquid/gas (90.03%) and oil/water (100%) separation efficiencies when compared to the other studied geometries.

**Keywords:** Simulation, VOF, Oil, Gas, Water.

## 1 Introduction

The separation of phases in fluids extracted from oil wells occurs in most cases in multiphase separators, which are pressure vessels located immediately after the wellhead and have the main objective of separating production into its gas, oil, and water phases. Separators can be classified according to the number of phases to be separated (biphasic and triphasic), orientation (vertical, horizontal, or spherical), and operating pressure (low, medium, or high). The appropriate selection of this equipment depends on various factors, such as fluid properties, available space for installation on platforms, potential operational problems due to the produced fluids, and the cost of design and development [1-3]. Therefore, various experimental and numerical studies are conducted aiming to mitigate operational issues in the separation process [4-6].

The use of three-phase horizontal separators stands out mainly for their operational ease in handling significant liquid flow rates (oil/water) and for providing better results in the presence of emulsions. This behavior is due to the horizontal length of the equipment, which allows for a larger interfacial separation area compared to vertical separators [7]. Despite the advantages, horizontal separators face operational challenges that reduce separation efficiency. These include forming recirculation zones, oil and water droplet entrainment by gas, gas bubble entrainment by the liquid phase, and level control and solid separation

issues. Numerous studies aim to optimize these separators' operational and geometric aspects, constantly seeking improvements in phase separation and, consequently, in reducing their dimensions and costs [8-17].

Yu et al. [18] and Oshinowo et al. [19] state that to improve separation efficiency and simultaneously reduce the overall vessel dimensions, different internal devices can be selected and installed to enhance gas/liquid and liquid/liquid separation. These devices significantly influence the fluid dynamics inside the equipment, mitigating operational issues.

Recent studies have demonstrated that the optimization of separation processes can also be achieved by incorporating novel internal devices such as corrugated plates. For instance, Oruç and Yayla [20] designed a corrugated plate system for crude oil-water mixtures, reporting a maximum separation efficiency of 99.6% through the optimization of parameters such as the ratio of the distances between plates to width, length to width ratio, the temperature values of the mixture before entering the separation system and the mounting angles of these plates in the separation system using the Response Surface Methodology (RSM).

In another study, Oruç and Yayla [21], developed a wastewater treatment system using corrugated plates based on gravitational separation to process an oil-water mixture. Both uncoated and hydrophobic-coated plates were tested, examining how parameters such as hole diameter, plate length, curvature angle, pumping speed, mounting angle, and plate

spacing affected the treatment capacity. To assess the impact of these factors and the hydrophobic coating, optimization was performed using the Response Surface Methodology (RSM) and Box - Behnken design. The results showed that treatment capacity was significantly influenced by flow dynamics, boundary layer thickness, and fluid energy changes. Additionally, the hydrophobic coating increased the treatment capacity and the mounting angle of the plate sets in the system greatly affected the treatment capacity.

Internal devices have different structural configurations, varying in geometric design, quantity, position, and function within separator vessels. Unlike external sizing, internal devices do not follow a standardized norm [22], and there is no consensus in the scientific community to establish a single optimized arrangement. These devices generally improve phase separation by optimizing inertial separation, reducing turbulence and recirculation zones, assisting in the agglomeration of liquid droplets, or retaining liquid droplets at gas outlets, thereby establishing a more uniform gas/oil/water separation.

Considering that turbulence and recirculation zones are issues that can affect the separation efficiency of separator vessels, the analysis of fluid velocity becomes indispensable. The fluid velocity distribution is an essential parameter in the study of horizontal separator vessels, especially in the gravitational separation region, where fluids are primarily separated by density difference under the influence of gravitational force. To favor sedimentation, fluids must establish a flow in the separation region with minimal turbulence, without recirculation zones, as they intensify mixing.

Higher velocities are observed during the fluid entry into the equipment, and the insertion of internal entry devices is a solution for inertial separation. Deflectors are examples of internal entry devices that seek to reduce turbulence along the separator vessel; they act to decrease fluid velocity, thereby increasing separation efficiency between phases Yayla et al. [23, 24], Nascimento [8], and Ghaffarkhah et al. [13,14] mainly evaluated the positioning and functionality of flat plate and semicircular deflectors. Liu et al. 2020 [25] studied the separation mechanism com deflectors vane-type. Yu et al. [18] and Kharoua et al. [26-28] studied deflectors with vane-shaped blades, perforated plates, and cyclones.

Regarding semi-perforated deflectors, the work of Yu et al. [18] stands out, in which they analyzed orifice plate deflectors under specific geometries and positions with porous vertical and horizontal rods. However, in the reported works, the situation where deflectors were geometrically constructed with a solid vertical rod and a porous horizontal rod was not evaluated.

Given the above, this research aimed to enhance the understanding of the impact of semi-perforated deflectors on flow dynamics and phase separation efficiency in a three-phase horizontal separator vessel. To achieve this purpose, computational fluid dynamics was employed to investigate how inserting an entry deflector with a solid vertical rod and

a perforated horizontal rod affects the separation between gas, oil, and water in a three-phase separator vessel. Additionally, we examined how the deflector's location influences the fluid behavior in the system.

## 2 Mathematical Modeling

For modeling the three-phase separator vessel, the fluids were considered incompressible, isothermal, and Newtonian under turbulent flow conditions. The Euler-Euler approach was employed to model the three-phase flow, and the Volume of Fluid (VoF) method was used for interface tracking with the sharp-dispersed algorithm. The governing equations include the continuity equation, the Navier-Stokes equation, and the  $\kappa - \varepsilon$  turbulence model.

The continuity equation can be formulated as:

$$\frac{\partial \rho}{\partial t} + \nabla \cdot (\rho \mathbf{u}) = 0 \quad (1)$$

where  $\rho$ , and  $\mathbf{u}$  are the density and velocity, respectively.

The momentum equation can be written as:

$$\begin{aligned} \frac{\partial(\rho \mathbf{u})}{\partial t} + \nabla \cdot (\rho \mathbf{u} \mathbf{u}) \\ = -\nabla p + \nabla \cdot \boldsymbol{\tau} + \rho \mathbf{g} + \mathbf{T}_\alpha \\ + S_p \end{aligned} \quad (2)$$

where  $p$  and  $\mathbf{g}$  are the gas pressure and gravitational acceleration terms, respectively. The term  $\boldsymbol{\tau}$  represents the stress tensor calculated by:

$$\begin{aligned} \boldsymbol{\tau} = (\mu_l + \mu_t)(\nabla \mathbf{u} + (\nabla \mathbf{u})^T) \\ - \frac{2}{3}(\mu_l + \mu_t)(\nabla \cdot \mathbf{u})\mathbf{I} \end{aligned} \quad (3)$$

where  $\mu_l$  and  $\mu_t$  are the laminar and turbulent viscosity, respectively. The turbulent viscosity is calculated using the Smagorinsky model, which for large turbulent structures are solved directly while small ones are modeled by:

$$\mu_t = C \rho_g \Delta^2 \sqrt{\left(\frac{\partial u_i}{\partial x_j} + \frac{\partial u_j}{\partial x_i}\right)^2} \quad (4)$$

where  $\Delta$  is the characteristic length, equal to the cube root of the volume of the element,  $\Delta = (\Delta x \Delta y \Delta z)^{1/3}$ .  $C$  is the Smagorinsky constant, given as 0.01.

The term  $\mathbf{T}_\alpha$  refers to the interfacial tension at the interface responsible for the coupling between phases. This force is given by Equation 5.

$$\mathbf{T}_\alpha = \sigma_{ij} \frac{\rho \zeta_i \nabla \alpha}{\frac{1}{2}(\rho_i + \rho_j)} \quad (5)$$

Where  $\sigma_{ij}$  is the interfacial tension term between phase  $i$  and phase  $j$ , and  $k_i$  is the local curvature. The term  $S_p$  models the porous regions present in the study domain and is given by Equation 6.

$$S_p = -\left(\frac{\mu}{\xi}\mathbf{u} + \frac{1}{2}C_F\rho\mathbf{u}|\mathbf{u}|\right) \quad (6)$$

Where  $\frac{1}{\xi}$  is the viscous resistance coefficient [ $\text{m}^2$ ] e  $C_F$  is the inertial resistance coefficient [ $\text{m}^{-1}$ ].

The Volume of Fluid (VoF) interface tracking algorithm allows for the assessment of detachment of the secondary phase and morphological changes concerning the continuous phase. To achieve this, it is assumed that the fluids are interpenetrating, such that the volume fraction must be between 0 and 1 ( $0 < \alpha_q < 1$ ), indicating the interface. The adopted equation to model this phenomenon is described in Equation 7.

$$\frac{\partial}{\partial t}(\alpha_q) + \nabla \cdot (\alpha_q \mathbf{u}_q) \quad (7)$$

The  $\kappa - \varepsilon$  model was used to simulate the effects of turbulence during the gas flow. The  $\kappa$  equation represents turbulent energy, while the  $\varepsilon$  equation represents the energy dissipation rate. Both equations are presented below.

$$\frac{\partial}{\partial t}(\rho\kappa) + \nabla \cdot (\rho\kappa\mathbf{u}) \quad (8)$$

$$= \nabla \cdot \left[ \left( \mu + \frac{\mu_t}{\varepsilon_\kappa} \right) \nabla \kappa \right] + G_\kappa + \rho\varepsilon_\kappa$$

$$\frac{\partial}{\partial t}(\rho\varepsilon) + \nabla \cdot (\rho\varepsilon\mathbf{u}) \quad (9)$$

$$= \nabla \cdot \left[ \left( \mu + \frac{\mu_t}{\varepsilon_\varepsilon} \right) \nabla \varepsilon \right] + \frac{\varepsilon}{\kappa} (C_1 G_\kappa - C_2 \rho\varepsilon)$$

In these equations,  $G_\kappa$  represents the generation of turbulence kinetic energy due to the mean velocity gradients, where  $C_1 = 1.44$  and  $C_2 = 1.92$ .  $\varepsilon_\kappa = 1.0$  and  $\varepsilon_\varepsilon = 1.3$  are the turbulent Prandtl numbers for  $\kappa$  and  $\varepsilon$ , respectively.

### 3. Simulation Setups

#### 3.1. Geometry and Mesh

This study was based on the industrial three-phase (gas/oil/water) separator belonging to the Abu Dhabi Company for Onshore Oil Operations (ADCO) investigated by Kharoua et al. [27-29]. Given the scarcity of geometric details, some simplifications were made to the internal structural arrangement. Only the weir and two perforated plates with 40% porosity were considered.

Efendioglu et al. [16] and Yayla et al. [17, 18] analyzed the effect of the positioning of a flat plate-type inlet deflector on the separation efficiency of an oil/gas two-phase separator. The authors found that, among the analyzed positions, when the deflector is located at a greater distance from the inlet, the separation efficiency increases. In turn, Yu et al. [14] identified, among the deflectors analyzed in a horizontal three-phase separator, that the flat plate-type deflector can cause the formation of primary vortices due to the reduced

flow area in the inlet region, which impairs separation efficiency. In light of this, aiming to evaluate whether these behaviors are observed or mitigated by the insertion of semi-perforated deflectors in a three-phase separator, two different configurations of baffles were proposed and analyzed, varying their distance from the inlet, height relative to the bottom of the vessel, and vertical length. The studied geometries are depicted in Figure 1.

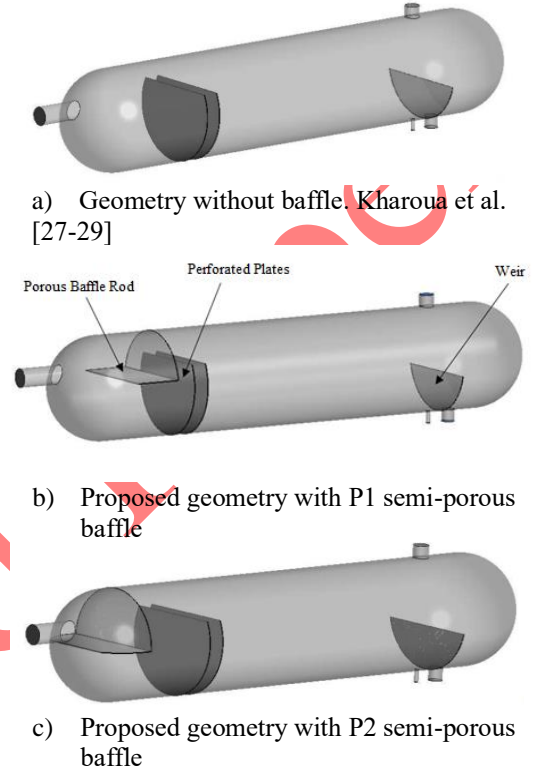


Fig 1. Geometry of the three-phase separator.

The main dimensions of the three-phase separator are presented in Table 1.

Table 1. Separator dimensions.

Region	Value [mm]
Vessel diameter (D)	3400
Vessel length (L)	14000
Inlet nozzle diameter	610
Gas outlet nozzle diameter	482,6
Oil outlet nozzle diameter	431,8
Water outlet nozzle diameter	139,5
Height of perforated plates	2450
Weir width	20
Weir height	1300

Source: Kharoua et al. [27, 28, 29]

These proposed internal devices are semi-perforated, and their dimensions are presented in Table 2.

Table 2 Deflector dimensions.

	Semi-porous P1 [mm]	Semi-porous P2 [mm]

Entrance distance	4990	3230
Height relative to the bottom of the vessel	2020	1750
Vertical length	1380	1650
Horizontal length	3339.22	3397.11
Width	1500	1500
Porosity	70%	70%

The accuracy of a CFD solution is directly influenced by the number of elements in the mesh. Generally, a larger number of elements leads to a finer mesh and, consequently, better simulation accuracy. However, increasing the mesh refinement also results in higher computational processing costs and longer calculation times. Therefore, it is recommended to perform a mesh dependency analysis for CFD studies. This analysis requires the mesh to be refined in stages until no significant differences in results occur between successive refinement stages. In this way, the results will be 'mesh-independent' [30]. Given this, this study performed a mesh independence test to determine the best balance between accuracy, stability, and computational cost. Additionally, the Grid Convergence Index (GCI) method proposed by Celik [31] was also used.

In the mesh independence test, the geometry of the separator with the P1 semi-porous baffle was discretized, generating four hybrid meshes that contain tetrahedral and hexahedral elements, as shown in Table 3. Based on the simulation results for the different meshes, a line was selected, created with the points  $(x=0.422995; y=0.86250; z=0)$  and  $(x=0.422995; y=1.26687; z=0)$ . The pressure variable was calculated along the selected line, and the result for each generated mesh was identified, as illustrated in Figure 2. The variation in results decreases as the number of mesh elements increases, until the influence of meshes 1 and 2 becomes small on the pressure result. In other words, additional mesh refinement did not cause significant

changes in the pressure result, and therefore, the results can be considered mesh-independent. Thus, considering the reduction in computational cost, the orthogonal and skewness mesh quality criteria, and the GCI analysis results, mesh 2 was selected, with 4,862,779 elements, as illustrated in Figure 3b. The geometries without a baffle and with the P2 baffle were discretized in a similar manner, using the same element size as mesh 2.

**Table 3** Mesh Independence Test.

Mesh	Number of Elements	Number of Nodes
Mesh 1	4943008	2431423
Mesh 2	4862779	2414919
Mesh 3	652658	204430
Mesh 4	118573	28588

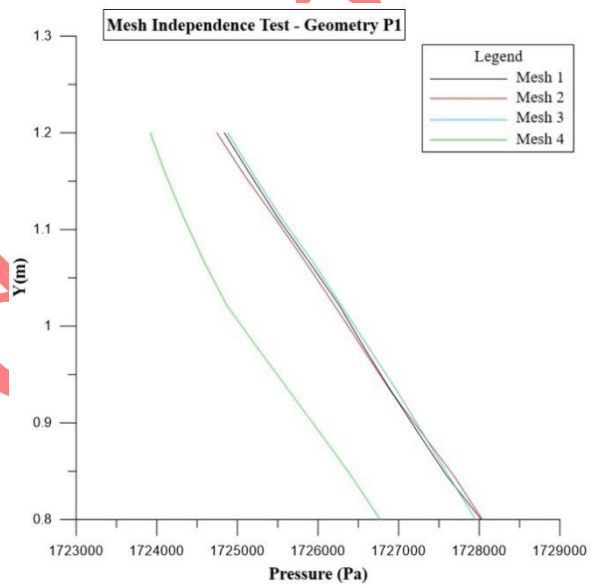
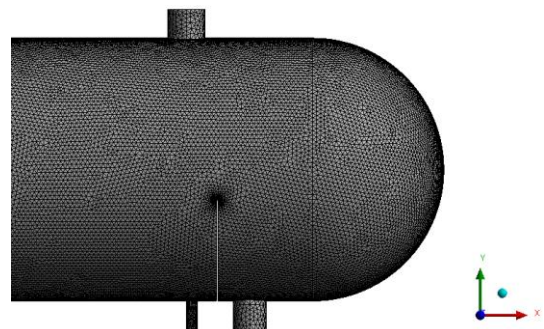


**Fig 2.** Mesh Independence Test.



(a-1) Enlargement of the input region.



(a-2) Enlargement of the separation region.

(a) Mesh of the geometry without baffle.

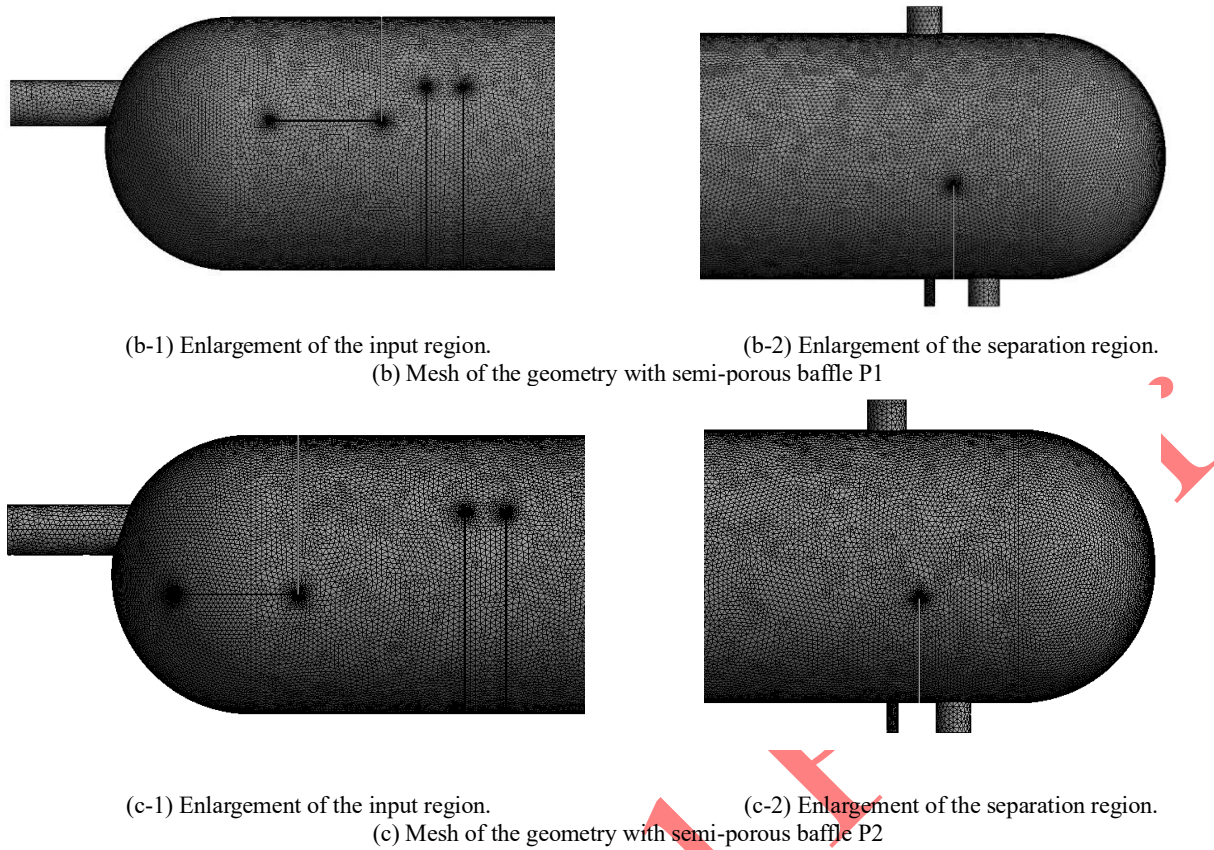


Fig 3. Numerical mesh

### 3.2 Boundary Conditions

The inlet and outlet boundary conditions are in accordance with those presented by Kharoua et al. [26-28], based on the industrial three-phase separator. In the three geometries analyzed in this study, the inlet condition consists of a multiphase mixture with a volumetric fraction of 92% gas, 6% oil, and 2% water. This mixture enters the three-phase separator with a velocity of 7.49 m/s. There are three outlets in the equipment, one for gas, another for oil, and the third for water, with imposed boundary conditions of 17.2 bar, 17.26 bar, and 17.38 bar, respectively. The initial liquid level in the separator vessels was obtained from a steady-state simulation that started with 50% liquid and 50% gas. After simulating for 1000 iterations, the result of this simulation was used as the initial condition for the transient study. Transient cases were simulated for 30 seconds and 180 seconds.

The separation efficiencies were calculated from the mass flow rates at the gas, oil, and water outlets, according to Equation 10. The inlet flow rates can be calculated from the inlet boundary conditions obtained from Kharoua et al. [26-28]. The geometric configuration that achieved the best separation result was simulated for 180 seconds.

$$\eta = \left( \frac{Q_{mafase_{inlet}} - Q_{mafase_{outlet}}}{Q_{mafase_{inlet}}} \right) \quad 10$$

The fluid properties used in the study are presented in Table 4.

Table 4 Properties of the materials.

Fluid	Density [kg/m <sup>3</sup> ]	Viscosity [kg/ms]	Superficial Tension [N/m]
Gas	17.58	1.1e-5	2.1e-2
Oil	813.46	2.3e-3	6.5e-2
Water	1015.10	1.1e-3	4.1e-3

Source: Kharoua et al. [26-28]; Ghaffarkhah et al. [13]

The baffles shown in the geometry of Figure 1 have a porosity of 40%, with isotropic viscous and inertial resistances of 21110000 m<sup>-2</sup> e 1822.1m<sup>-1</sup>, respectively.

The equations were solved using the finite volume method (FVM). In this approach, the transient term was discretized using the second-order Crank-Nicolson scheme, while the convection and diffusion terms were discretized using the Upwind schemes. These discretization schemes were chosen because they demonstrated numerical stability in solving the linear matrix.

The result of the discretization is a set of algebraic equations constructed in the form  $A\phi = b$ . The coefficients of the unknown variables in matrix  $A$  are obtained through the linearization procedure of the information within the computational mesh. Vector  $b$  contains all the source terms, including constants, boundary conditions, and non-linearizable components. The techniques for solving this algebraic system are not dependent on the specific discretization method employed. In this study, the GAMG method was used

for solving the pressure field, the smoothSolver for the velocity field, and the PBICGStab for the other fields.

## 4 Results

### 4.1 Fluid behavior

#### 4.1.1 Geometry without the baffle - Case 01

Results of the gas, oil, and water volumetric fraction fields from simulations of the geometry without the baffle of the separator vessel were obtained, as indicated by Figures 4-6. The volume fraction contours also illustrate the presence of gas primarily in a mixture with oil, highlighting the regions upstream of the first deflector in a zone of more significant mixing. The perforated plates do not fully contain this mixture and propagate immediately downstream of the second porous plate, as seen in the flow lines in Figure 7. The intense mixing between phases in the entry region, located upstream of the perforated plates and also known as the mixing region, when not dissipated in the separation region, contributes to reducing the efficiencies of liquid/gas and liquid/liquid separation. This occurs because more liquid may exit at the gas outlet, as well as water at the oil outlet and oil at the water outlet.

The separation region encompasses the entire horizontal area downstream of the second perforated plate. At 30 seconds, a water mass flow rate of 15.95 kg/s was identified at the gas outlet. The action of the upper part of the plates causes water displacement in the form of overflow, allowing it to position itself above the oil layer at the oil and gas interface. Consequently, this contributes to its entrainment at the gas outlet. This effect can be visualized in the water volumetric fraction contours (Figure 6) and through the vectors (Figure 8).

Gas phase volume fraction

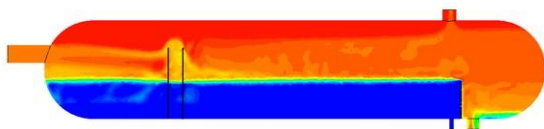


Fig 4. Gas volumetric fraction.

Oil phase volume fraction

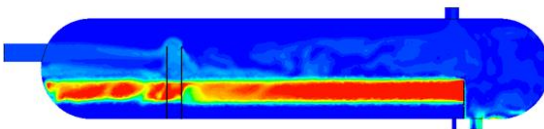


Fig 5. Oil volumetric fraction.

Water phase volume fraction

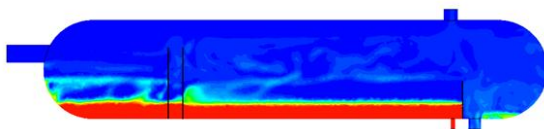


Fig 6. Water volumetric fraction.

Velocity [m s<sup>-1</sup>]

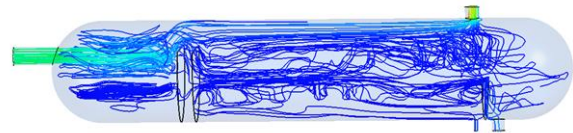


Fig 7. Streamlines of the mixture.

Velocity [m s<sup>-1</sup>]



Fig 8. Velocity vector field.

The total liquid mass flow rate at the gas outlet was 27.21 kg/s. The presence of water above the oil layer also contributes to the discharge of this fluid along with the oil, as the weir generates an overflow effect that directs water toward the oil outlet. The mass flow rate of water at the oil outlet reached 14.19 kg/s simultaneously.

#### 4.1.2. Geometry with the semi-porous baffle P1 – Case 02

When comparing the results obtained from the geometry with the semi-porous baffle P1 to the case without a baffle, it can be observed from the volumetric fraction contours of gas, oil, and water (Figures 9, 10, 11) that the dispersion of liquid in the separation region in the upper gas zone (separation region) was considerably reduced, favoring the gas/liquid separation efficiency. The reduction in liquid dispersion in the gas indicates that the gas may entrain less liquid. In this case, the liquid mass flow rate at the gas outlet was 14.98 kg/s, while in the case without a baffle, it was 27.21 kg/s. Among the liquid components, the water showed higher flow rates at the gas outlets, 15.95 kg/s for the case without a baffle and 8.95 kg/s for the case with a semi-porous baffle P1.

The presence of gas in the mixing zone upstream of the first perforated plate (Figure 9) is minimized compared to the case without a baffle. There is also a reduction in mixing in the oil layer immediately after the second perforated plate (Figure 10). The oil layer appears more uniform and thinner compared to the case without a baffle. The reduction in thickness is related to more oil exiting at the oil outlet and less oil present at the gas outlet. An oil flow rate of 62.47 kg/s is obtained for the case with semi-porous baffle P1, while only 54.89 kg/s exits at the oil outlet for the case without the baffle. In the gas outlet, there are 11.25 kg/s of oil in the case 01 and only 6.04 kg/s in the case 02.

On the other hand, the water layer (Figure 11) has a greater thickness than case 1. However, the final liquid level remains uniform in both cases. In the absence of the baffle, the water flow rates through the oil and gas outlets are 14.1918 kg/s and 15.95 kg/s,

respectively, while in the case with the presence of semi-porous baffle P1, these values become 12.34 kg/s and 8.95 kg/s, respectively. On the other hand, more water exits through its respective outlet in the case without a baffle, at a flow rate of 19.77 kg/s, justifying the reduction in the level compared to the case with the semi-porous baffle P1.

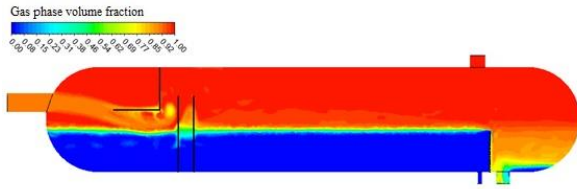


Fig 9. Gas volumetric fraction.

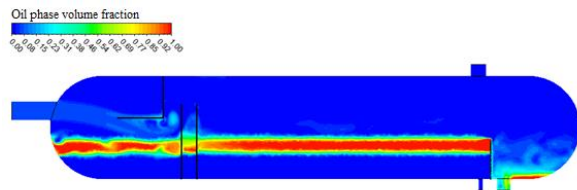


Fig 10. Oil volumetric fraction.

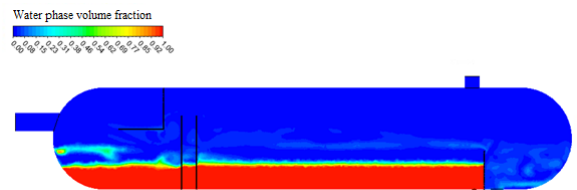


Fig 11. Water volumetric fraction.

When fluids enter the equipment, they encounter the semi-porous baffle, and a portion of the flow initially collides with the horizontal perforated plate and subsequently with the solid vertical plate, recirculating upstream of it (Figure 12). Another portion of the flow moves beneath the semi-porous baffle and collides with the first perforated plate, then recirculates between it and the solid back of the semi-porous baffle. The combined action of the baffle and plates allows the velocity to dissipate more in the mixing region (Figure 12).

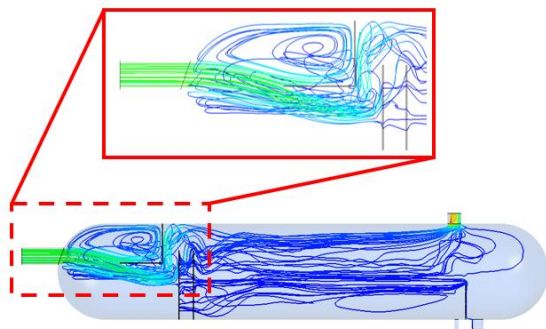


Fig 12. Streamlines of the mixture.

From the velocity fields (Figure 13), it can be observed that successive collisions with the baffle and porous plate lead to a decrease in phase velocities,

thereby reducing momentum in the entry region, which then increases again at the gas outlet. As a result, the vertical velocity is reduced in front of the first porous plate, and consequently, less liquid is dispersedly entrained in the upper part of the vessel.

Regarding the flow lines in the liquid layers in the separation region (Figure 12), it is noticeable that they are more stable when compared to the case without a baffle (Figure 7). It is essential to highlight that the flow lines indicate that the height of the plates contributes to a displacement of fluids towards the upper gas zone. In situations of higher velocities, the liquid ends up being more entrained.

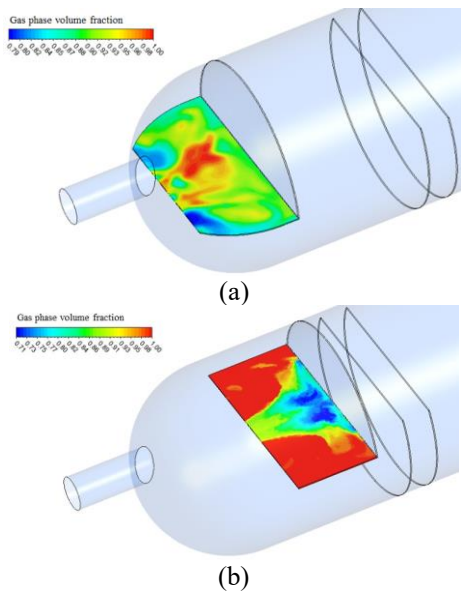


Fig 13. Velocity contours of the phases.

#### 4.1.3. Geometry with the semi-porous baffle P2 – Case 03

With the results from the simulation of the geometry with semi-porous baffle P2, a reduction in the free area for the settling of part of the fluids is observed as the baffle approaches the equipment inlet. The fluids recirculate after successive collisions with the solid vertical rod of the baffle, with some flowing through the porous horizontal plate and others descending beneath the baffle. In cases 02 and 03, both semi-porous baffle are responsible for inertial separation. The difference in momentum of the phases allows the less dense phase to continue recirculating for longer while the denser phases settle. However, the reduction in the free area in front of the deflector hinders the immediate settling of the liquid phases, coupled with the resistance caused by the 70% porosity in the horizontal part of the baffle, contributing to more significant mixing with the gas compared to the case with semi-porous baffle P1. As they cross the porous horizontal plate, the mixture between the liquid and gas phases can be visualized in the gas volume fraction contours (Figure 14).

Compared to the case 02, the approach of the baffle to the inlet impaired separation, especially of the liquid phases. As part of the free water, a term used when the water phase is separated from the oil in its stratified form tends to settle upon entering the vessel, even before crossing the baffle. This is possible because there is a reduction in velocity during expansion caused by the difference in cross-sectional area between the inlet pipe and the diameter of the vessel, allowing some liquid/gas separation even in the absence of an inlet baffle. Therefore, the semi-porous baffle P1 case exhibits less mixing, as the baffle is positioned at a distance from the inlet that allows an intermediate action of the processes experienced by the case without a baffle and the case with semi-porous baffle P2, resulting in greater liquid/gas separation.



**Fig 14.** Gas volumetric fraction on the semi-porous baffle (a) P2 (b) P1.

In light of the above, although there is a reduction in fluid inlet velocity, the intense mixing caused by recirculation under the baffle's positioning persists in the oil layer and gas region (Figures 15 and 16). It will result in changes in separation efficiency and liquid levels in the vessel. It is also noteworthy that internal devices such as mist extractors were not modeled to evaluate the phenomena of particle agglomeration and coalescence, which could favor the reduction of liquid at the gas outlet. Thus, for 30 seconds, there are 14.26 kg/s and 17.09 kg/s of water and oil at the gas outlet, respectively. In the case 01, the water and oil flow rates at the gas outlet are 15.95 kg/s and 11.25 kg/s, respectively. In turn, in the case 02, liquid is reduced at the gas outlet, reaching only 8.95 kg/s of water and 6.02 kg/s of oil.

The reduction in the water level in the case 03 results from water having a lower mass flow rate at the inlet, leading to more significant mixing with the oil and gas phases after crossing the baffle. Even though it is the denser phase, it will have difficulty settling due to entrainment, favoring its more significant presence at the gas and oil outlets. The presence of water above the oil layer (Figures 15 and 17) results in a less defined oil/gas interface compared to the case of semi-porous baffle P1, contributing to 19.18 kg/s of water exiting at the oil outlet, compared to 14.19 kg/s in the case without a baffle and 12.34 kg/s in the semi-porous baffle P1 case. Thus, the case of semi-porous baffle P2 presented the highest water flow rates at the oil outlet, as well as the highest liquid flow rates at the gas outlet, compared to the other two studied scenarios.

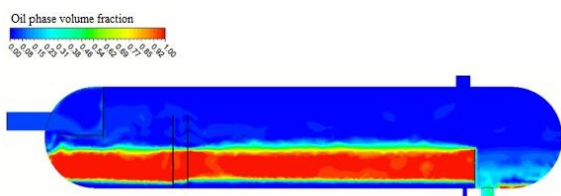


**Fig 15.** Oil volumetric fraction.

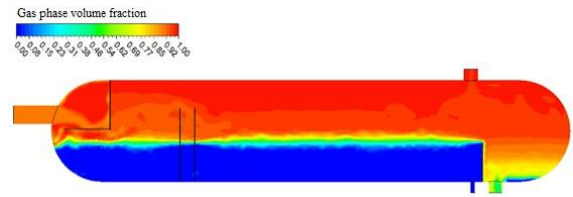


**Fig 16.** Gas volumetric fraction.

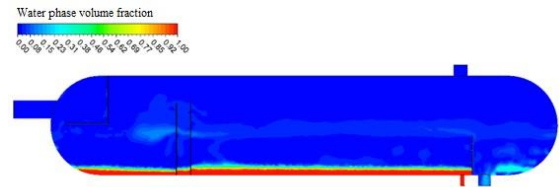


**Fig 17.** Water volumetric fraction.

## 4.2. Separation efficiency

Based on the water, oil, and gas flow rates at different outlets of the three-phase separator, as discussed and presented in Section 4.1, and utilizing Equation 10, the separation efficiencies were calculated for the three evaluated geometric configuration scenarios. The results are presented in Table 6. Case 2, which represents the geometry with the P1 semi-porous baffle, showed higher water/oil, oil/gas, water/gas, and liquid/gas separation efficiencies compared to cases 1 and 3. These results indicate that the insertion of the P1 baffle influences fluid separation, reducing the presence of liquids in the gas outlet, as well as the presence of water in the oil outlet, when compared to the cases without a baffle and with the P2 semi-porous baffle. Regarding the oil and water separation efficiency, all three cases present good results, with oil being present in the water outlet only in case 3.

For the evaluation of the applied mathematical model and the numerical simulations performed with the insertion of the proposed semi-perforated devices, the separator vessel's separation efficiency data can be compared with experimental data (ADCO performance test results) from the Bab field in Abu Dhabi by the ADCO company, as presented by Kharoua et al. [26] and available in Table 5, since the operational conditions and the simulated equipment geometry were based on the same study.

**Table 5** – Comparison of results

	Oil/water (ppm)	Water/gas (USG/mm scfd)	Oil/gas (USG/mm scf)
ADCO performance test results*	≤ 2000	≤ 0.1	
Case 2 (Baffle P1)	0	0.38	0.32
Case 3 (Baffle P2)	705.44	0.63	0.93

Source: \*Adaptado de Kharoua et al. [28]

As shown in Table 5, for the numerical analyses performed in this article with 30 seconds of simulation,

no oil was found in the water outlet in case 2, while in case 3, the oil concentration was 705.44 ppm. In this sense, the numerical results meet the performance metric expected in the experimental test of the ADCO three-phase separator, regarding the presence of oil in the water outlet, as both case 2 and case 3 present concentration values below 2000 ppm. Although the objective of this analysis is purely comparative, due to the lack of information on the exact time of obtaining the results in the experimental test presented in Kharoua et al. [28] and considering the simplifications made in the simulated geometries, it is important to highlight that the presented data contribute to the validation of the general operation of the equipment, especially since the simulation results meet one of the expected performance metrics for analyzing the separation efficiency in the three-phase separator vessel. On the other hand, although the simulation results do not meet the concentration values of liquid lower than 0.1 USG/mmscf in the gas outlet, as indicated by the experimental test, the results can be considered acceptable, since coalescer and mist extractor devices were not modeled in the simulated geometries, and these are responsible for reducing liquid carryover in the gas, which may influence the outcome. Finally, it is worth noting that, for both simulated results, case 2 shows values closer to those expected in the experimental performance test when compared to case 3.

#### 4.3. Behavior of phases in the scenario of geometry with baffle P1

According to Stewart and Arnold [1], for gas/liquid and liquid/liquid separations to occur in a three-phase separator vessel, the expected residence time varies between 1-3 minutes and 3-30 minutes, respectively. In this sense, due to existing computational

limitations, an initial analysis was carried out considering 30 seconds of simulation, mainly to evaluate the dynamic behavior of the phases inside the equipment. After that, a simulation was performed for 180 seconds in order to meet the minimum settling time for the separator vessel estimated in the literature and to calculate the separation efficiencies obtained in the studied cases. With the obtained results and using Equation 10, the separation efficiencies were calculated for the 3-minute simulation. Thus, as indicated by the initial results in Table 6, after 180 seconds of simulation, the separator with the P1 semi-perforated baffle (case 2) continued to show the highest separation efficiencies when compared to the separator vessels without a baffle (case 1) and with the P2 semi-perforated baffle (case 3). In this sense, the results of separation efficiency over time for the geometry with the P1 semi-porous baffle are presented in Table 7, and the behavior of the volumetric fractions of water, oil, and gas for this geometry is presented in Figures 18–20.

When analyzing Table 6 and Figures 18-20, it can be observed that the equipment has not yet reached equilibrium, and the flow behavior varies between 50 and 180 seconds. To understand the effect of the deflector P1 on the oil layer at 180 seconds, the results of geometry without the baffle and com semi-porous baffle P2 are presented in Figure 21.

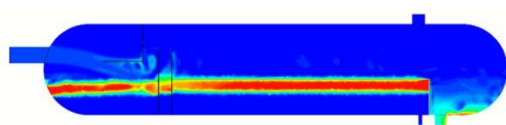
By comparing the results of the different geometries shown in Figure 21, a considerable reduction in the presence of oil in its dispersed phase in the gas phase can be observed for the geometry with the semi-porous baffle P1, which may have contributed to the higher gas/liquid separation efficiency results.

**Table 6** - Separation efficiencies in the evaluated geometries.

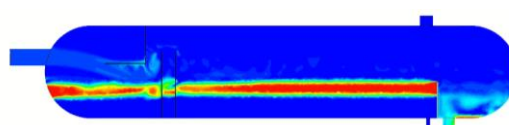
Case	Water/Oil (%)	Oil/Water (%)	Oil/gas (%)	Water/Gas (%)	Liquid/Gas (%)
01	67.86	100	89.39	63.87	81.90
02	72.03	100	94.32	79.71	90.03
03	56.56	99.99	83.90	67.71	79.14

**Table 7** - Separation efficiency over time for the case of semi-porous baffle geometry P1.

Time	Oil/Gas (%)	Water/Oil (%)	Oil/Water (%)	Water/Gas (%)	Liquid/Gas (%)
50s	92.432	63.147	100	82.021	89.374
100s	90.912	75.760	100	85.553	89.338
150s	90.912	75.760	100	85.553	89.338
180s	89.820	67.357	100	86.885	88.958
Average	91.019	70.506	100	85.003	89.252



50s



100s

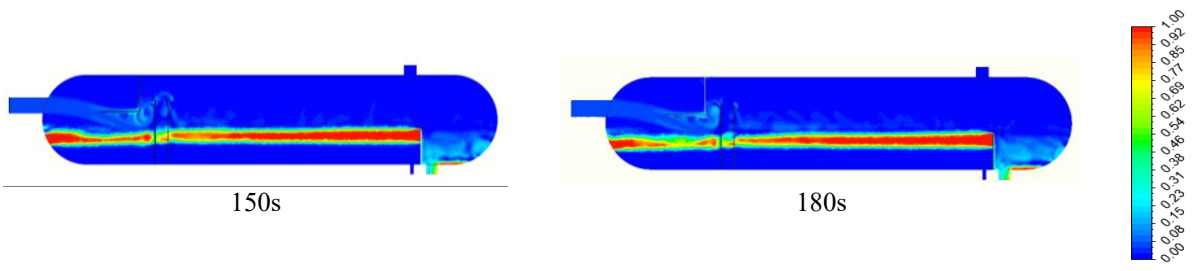


Fig 18. Oil volumetric fraction.

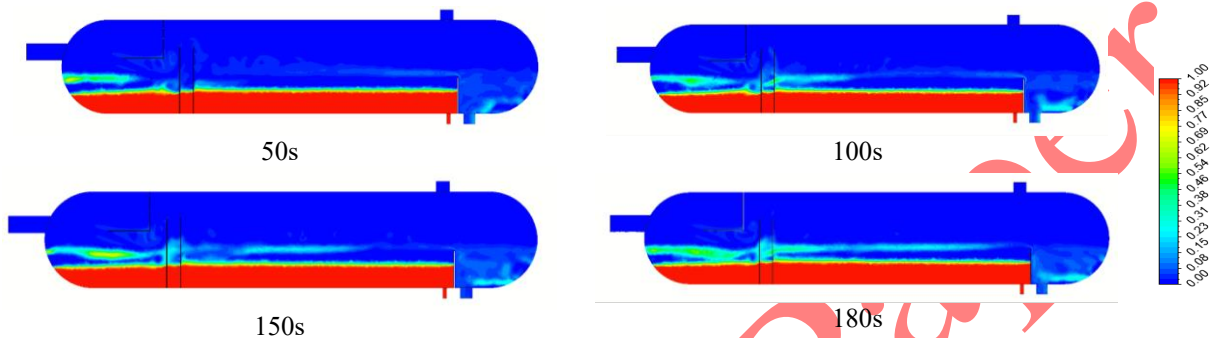


Fig 19. Water volumetric fraction.

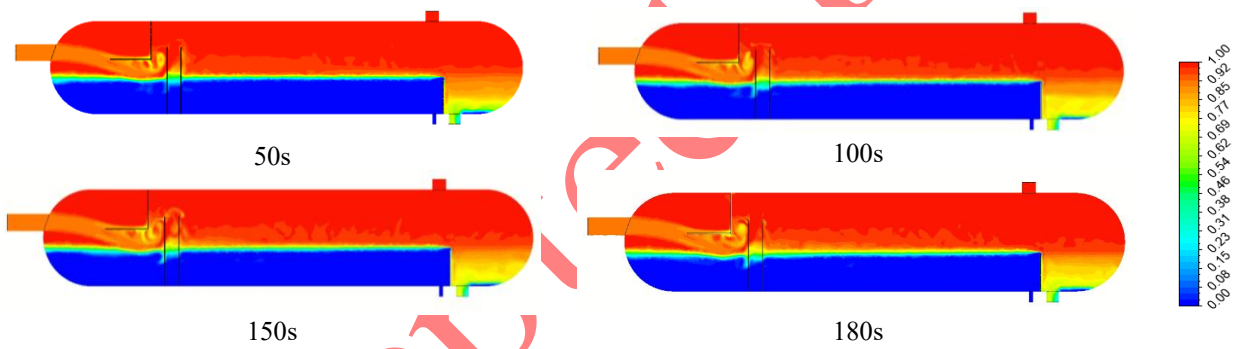


Fig 20. Gas volumetric fraction.

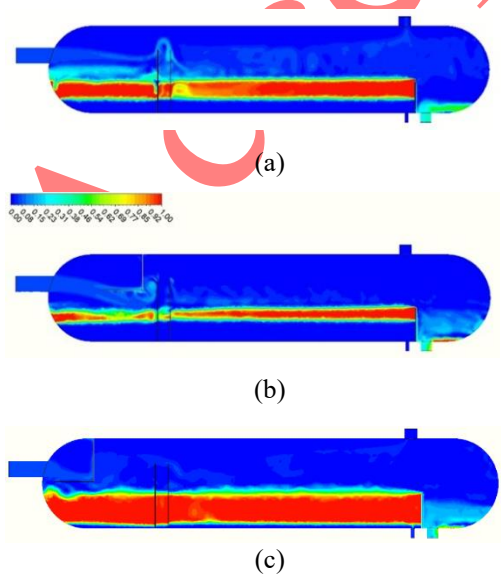


Fig 21 – Oil volumetric fraction at 180 seconds. (a) Without deflector (b) Semi-porous deflector P1 (c) Semi-porous deflector P2.

## 5 Conclusion

Based on the numerical simulation, the mathematical modeling developed with the VOF (Volume of Fluid) multiphase model with a sharp/dispersed interface and the standard  $k-\epsilon$  turbulence model physically describes the fluid dynamic behavior of gas, oil, and water during the phase separation process in the horizontal separator vessel. The action of perforated plates contributes to attenuating the mixture velocity at the inlet. It also highlights recirculation zones upstream, downstream, and between them, in addition to favoring liquid entrainment by gas. The insertion of semi-porous entry baffle P1 and P2 attenuates the velocity of incoming fluids compared to the separator vessel without an inlet baffle. The separation efficiencies obtained vary according to each inserted device. The semi-porous baffle P1 yielded the best results regarding separation efficiencies for water/oil (72.03%), oil/water (100%),

oil/gas (94.32%), water/gas (79.71%), and liquid/gas (90.03%) when compared to cases with geometries without a baffle and with semi-porous deflector P2. It can be concluded that the three-phase horizontal separator equipped with a semi-porous entry baffle P1, with two perforated plates and a weir, presents promising results for the three-phase separation of gas, oil, and water under the analyzed inlet conditions.

## NOMENCLATURE

$\mathbf{u}$	Velocity vectors [m/s]
$\rho$	Density [kg/m <sup>3</sup> ]
$p$	Pressure [Pa]
$\boldsymbol{\tau}$	Stress tensor [Pa]
$\mathbf{g}$	Gravity acceleration [m/s <sup>2</sup> ]
$\mathbf{T}_\alpha$	Continuum surface force [N/m <sup>2</sup> s <sup>2</sup> ]
$S$	Momentum source term [kg/m <sup>2</sup> s <sup>2</sup> ]
$\mu$	Dynamics viscosity [Pa s]
$\boldsymbol{\tau}$	Stress tensor [Pa]
$C$	Smagorinskyn [ ]
$\zeta$	Local curvature [1/m <sup>2</sup> ]
$\alpha$	Volumetric fraction [ ]
$\sigma$	Superficial tension [N/m]
$1/\xi$	Viscous resistance [m <sup>2</sup> ]
$C_F$	Inertial resistance [1/m]
$\kappa$	Turbulent energy [m <sup>2</sup> /s <sup>2</sup> ]
$\varepsilon$	Energy dissipation rate [m <sup>2</sup> /s <sup>3</sup> ]

## Subscripts

I	Phase i
J	Phase j
L	Laminar
Q	Mixture model
P	Porous

## References

- [1] M. Stewart, K. Arnold Elsevier, vol. 1, 2008.
- [2] M. Bothamley, J. M. Campbell Oil Gas Facil, vol. 2, pp. 21-29, 2013a.
- [3] M. Bothamley, J. M. Campbell Oil Gas Facil, vol. 2, pp. 35-47, 2013b.
- [4] T. T. Le, S. I. Ngoa, Y. Lima, C. Prrkb, B. Leeb, B. Kimb, D. Limc Journal of Petroleum Science and Engineering, 2018.
- [5] M. Oshinowo, R. D. Vilagines Chemical Engineering Research and Design, 2020.
- [6] Y. Shi, J. Chen, H. Meng Journal of Petroleum Science and Engineering, 2022.
- [7] S. Mokhatab, J. G. Speight, W. A. Poe Elsevier, 2006.
- [8] J. B. D. S. D. NASCIMENTO Master's thesis, UFCG, 2017.
- [9] N. Scapin, L. Cadei, M. Montini, G. Montenegro, A. Bianco, S. Mais 13 th Offshore Mediterranean Conference and Exhibition in Ravenna, 2017.
- [10] B. A. McCleney, A. R. Owston, T. S. Green, F. Viana, M. S. Nelson Offshore Tecnology Conference, 2017.
- [11] B. A. McCleney, T. S. Green, A. R. Owston Offshore Tecnology Conference, 2018.
- [12] A. Ghaffarkhah, A. M. Shahrabi, K. M. Moraveji, H. Eslami Egyptian Journal of Petroleum, vol. 26, pp. 413-420, 2017.
- [13] A. Ghaffarkhah, A. M. Shahrabi, K. M. Moraveji SPE production & operations, vol. 33, pp. 879-895, 2018.
- [14] A. Ghaffarkhah, A. Z. Dijvejin, A. M. Shahrabi, K. M. Moraveji, M. Mostofi Journal of Petroleum Exploration and Production Technology, vol. 9, pp. 353-382, 2019.
- [15] T. Ahmed, P. A. Russel, F. Hamad, S. Gooneratne Society of Petroleum Engineers Production & Operations, vol. 34, pp 805-819, 2019.
- [16] T. Acharya and L. Casimiro Journal of Ocean Engineering and Science, vol. 5, pp. 261-268, 2020.
- [17] T. Ahmed, P. A. Russel, F. Hamad, S. Gooneratne Heliyon, 2020.
- [18] P. Yu, S. Liu, Y. Wang, W. Lin, Z. Xiao, C. Wang International Conference on Advances in Computational Modeling and Simulation, 2012.
- [19] Oshinowo, L.; elsaadawy, E.; vilagines, R. CFD modeling of oil-water separation efficiency in three-phase separations. 10th International Conference on CFD in Oil and Gas, Metallurgical and Process Industries SINTEF. Norway. 2014.
- [20] M. Oruç, S. Yayla Separation Science and Technology, 2021.
- [21] M. Oruç, S. Yayla Journal of Environmental Engineering, 2023.
- [22] A. Efendioglu, J. Mendez, H. Turkoglu WIT Transactions on Engineering Sciences, vol. 82, pp. 133-142, 2014.
- [23] S. Yayla, K. Kamal, S. Bayraktar, M. Oruc International Journal of Mechanical And Production Engineering, 2017.
- [24] S. Yayla, K. Kamal, S. Bayraktar Journal of Applied Fluid Mechanics, vol. 12, pp. 1037-1045, 2018.
- [25] S. Liu, J. Zhang, L. Wang, J. Xu Separation and Purification Technology, 2020.
- [26] N. Kharoua, L. Khezzar, H. Saadawi SPE Annual Technical Conference and Exhibition, Society of Petroleum Engineers, pp. 8–10, 2012.
- [27] N. Kharoua , L. Khezzar, H. Saadawi Abu Dhabi international petroleum conference and exhibition. Society of Petroleum Engineers, 2012.
- [28] N. Kharoua, L. Khezzar, H. Saadawi ASME Fluids Engineering Division Summer Meeting, 2013.
- [29] N. Kharoua, L. Khezzar, H. Saadawi American Journal Of Fluid Dynamics, vol. 1, pp.101-118, 2013.
- [30] H. K. Versteeg, W. Malalasekera Longman Scientific & Technical, 1995.
- [31] I. B. Celik. Journal of Fluids Engineering, v. 130, n. 7, p. 078001-078001-4. ISSN 0098-2202.

Accepted Paper